Porosity control in 316L stainless steel using cold and hot isostatic pressing

Essa, Khamis; Jamshidi, Parastoo; Zou, Ji; Attallah, Moataz M.; Hassanin, Hany

DOI:
10.1016/j.matdes.2017.10.025

Document Version
Peer reviewed version

Citation for published version (Harvard):
Essa, K, Jamshidi, P, Zou, J, Attallah, MM & Hassanin, H 2018, 'Porosity control in 316L stainless steel using cold and hot isostatic pressing', *Materials and Design*, vol. 138, pp. 21-29. https://doi.org/10.1016/j.matdes.2017.10.025

Porosity Control in 316L Stainless Steel using Cold and Hot Isostatic Pressing

Khamis Essa[1]*, Parastoo Jamshidi[2], Ji Zou[2], Moataz M. Attallah[2], Hany Hassanin[3]

[1*]School of Engineering, University of Birmingham, UK, Email:k.e.a.essa@bham.ac.uk

[2]School of Metallurgy and Materials, University of Birmingham, UK

[3]School of Mechanical and Automotive Engineering, Kingston University, UK

Abstract

Porous biomedical implants are known for their improved osseointegration due to the ingrowth of bone tissues, combined with a lower elastic modulus to solid implants, resulting in a reduced likelihood for stress shielding and implant loosening. In this work, the control of the porosity content in capsule-free powder hot isostatic pressing (CF-HIPing) of 316L stainless steel was investigated. The proposed approach utilises cold isostatic pressing (CIPing) to form green compacts using rubber moulds, followed by CF-HIPing under suitable conditions. Porosity control was attained via the selection of the powder particle size used in creating the green compacts. The microstructural and mechanical properties development of the CF-HIPed structures was studied using optical and scanning electron microscopy, micro-computer tomography, hardness, and compression testing. The occurrence of powder necking was visualised using electron backscattered diffraction. The results showed a significant increase in the pore fraction of the samples with increasing the particle size of the powder. However, increasing the particle size was also associated with a drop in the elastic modulus, compressive strength, ductility, and hardness of the final structures. Nonetheless, porous structures with elastic modulus between 17-30 GPa were successfully produced using a powder particle size range of 32-50 μm, matching the elastic modulus of human bones.

Keywords: Hot Isostatic Pressing; Cold Isostatic Pressing; Porous Material; Austenitic stainless steel; Microtomography

1. Introduction

To-date, stainless steel has been the most widely used material in the medical implant sector, especially in producing orthopaedic implants and many other biomedical devices, including plates for fractured bones, fixtures, dental posts, and screws [1]. Its excellent biocompatibility, mechanical properties (strength and ductility,) and crevice and pitting corrosion resistance are attributed to the presence of Cr and Mo [2-4]. Nonetheless, the Young's modulus of 316L stainless steel (SS) is ~193 GPa, compared to 10-30 GPa for human bone, making the implants susceptible to failure due to stress shielding (i.e. the Young's modulus mismatch between the bone and implant) [5], as well as due to the weak bonding between the solid implant and the surrounding tissues [6]. As such, the development of highly porous stainless steel implants could be one of the approaches to address these concerns, by tailoring the density and hence the stiffness of the implant to match the bone's stiffness [7]. Furthermore, a porous implant offers a good biological environment to efficiently transport body fluids or drugs through the open porosity network, and allowing body tissues to grow. This provides an outstanding interfacial bonding between the implant and natural bone, enhancing the osseointegration [8].

Development of new processes to manufacture highly porous materials to address the aforementioned challenges has been growing rapidly, especially within the last decade. Conventional sintering of compacted powders is one of the approaches that have been used to manufacture parts with a very fine porosity. However, the sintered parts often have a lower mechanical strength, compared to that of a solid material. Furthermore, it can be difficult to control size, interconnectivity, and shape of the pores in sintering-based processes [1]. Foaming agents or space holder particles to create porous structures have also been investigated [9, 10]. Nonetheless, residual contaminations and impurities after consolidation restrict the use of this method in biomedical implants, where the use of alloys with extra low interstitials powders is typically sought. Additive manufacturing, freeze casting and injection moulding were also investigated in the production of structures with porosity ranging 55 %-86% [11-13].

Hot Isostatic Pressing (HIPing) is manufacturing process where parts or encapsulated powder compacts are subjected to high temperature and pressure simultaneously in a pressurised cylinder [14]. It has been extensively used in the medical industry to improve the mechanical properties of cast titanium, cobalt chrome and stainless steel 316L implant parts [15]. In powder HIPing, the powder is encapsulated in a canister of a desired cavity, but typically larger to compensate the

shrinkage the densification process. Still, the densification process is fairly non-uniform due to the interaction between the typically solid-walled capsule and the powder [14], as concluded by Kim and Jeon who used a stainless steel capsule to HIP stainless steel 316L powder, which resulted in an inhomogeneous deformation [16]. Although a number of computational tools for the shrinkage and densification have been developed to enable the design of the tooling [17-19], the elimination or the simplification of the encapsulation process (e.g. by using pre-sintering) is likely to simplify the process and reduce its cost.

In this paper, capsule-free HIPing (CF-HIPing) is employed to manufacture porous stainless steel 316L structures that can potentially be used in low-stiffness implants. The approach involves using powder Cold Isostatic Pressing (CIPing) in soft moulds to form the green compacts, followed by consolidation using HIPing without using a capsule. Effect of the particle size on the porosity, the mechanical and microstructural properties of the developed parts are also investigated using various microstructural and mechanical properties characterisation techniques.

2. Materials and Experimental Methods

A. Powder and CIPing

Gas atomised 316L stainless steel powder was supplied by Sandvik Osprey, UK. The powder was received into four different mean particle sizes (D50) of 5 μm, 10 μm, 16 μm and 50 μm (supplier's data). The composition is listed in Table 1, based on the supplier's composition data. The SEM images of the powder morphology were characterised using Scanning Electron Microscopy. As shown in Figure 1-(a,b,c,d), the particles have a spherical morphology in the various sizes, which helps produce a high packing density due to the ease of powder flow.

Table 1: composition of a supplied stainless steel 316L powders

Element	Fe	Cr	Ni	Mo	Mn	Others
Percentage	Balance	16.5	10.5	2.1	1.45	0.88

Polydimethylsiloxane (PDMS), a widely used silicon rubber material that transfers water pressure

efficiently, was used to fabricate soft moulds with cavities for the CIPing step. A PDMS kit (Sylgard 184-Dow Corning Corp.) consisting of (a base material and a curing agent) was used to fabricate the mould. A master mould that consists of plastic flat substrate holding glass cylinders was placed into an aluminium container as shown in Figure 2-a. The two parts were stirred together in a beaker with a weight ratio of 10:1, and de-gassed to remove the bubbles. After de-gassing, the prepared mixture was poured onto the mould and placed in a vacuum chamber again until all remaining bubbles were disappeared as shown in Figure 2-b. The mould was cured at 70 °C for 3 hours. After cooling down to room temperature, the cured PDMS mould was peeled off from the master mould as shown in Figure 2-c. In the preparation of the CIPed compacts, the soft moulds were filled with the as-received powders using a vibratory table to achieve a good packing density. Next, the moulds were covered from the top by a PDMS lid, sealed inside a rubber bag, and placed into the CIP cylinder, prior to pressurising the CIP to a pressure of 60 MPa. After releasing the pressure, the rubber bag was removed to extract, the CIPed compacts (see Figure 2-d), whose bulk density of the samples was calculated using the mass to volume ratio.

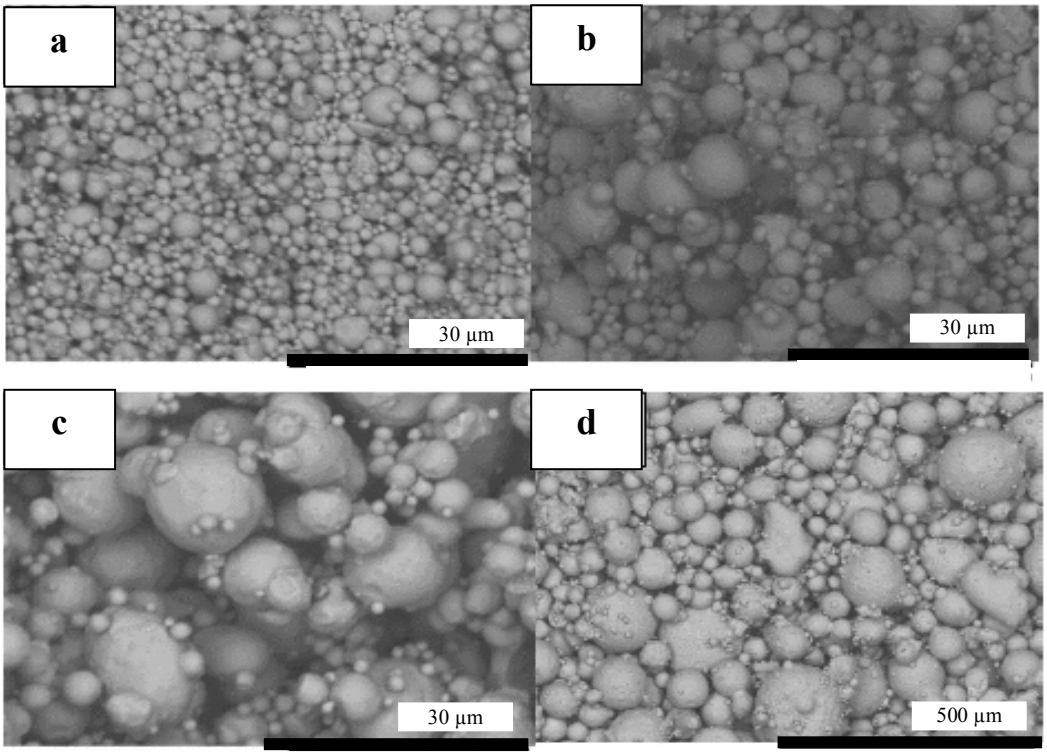

Figure 1. SEM images of the stainless steel powder with a mean size of (a) 5 μm, (b) 10 μm, (c) 16 μm, and (d) 50 μm, respectively.

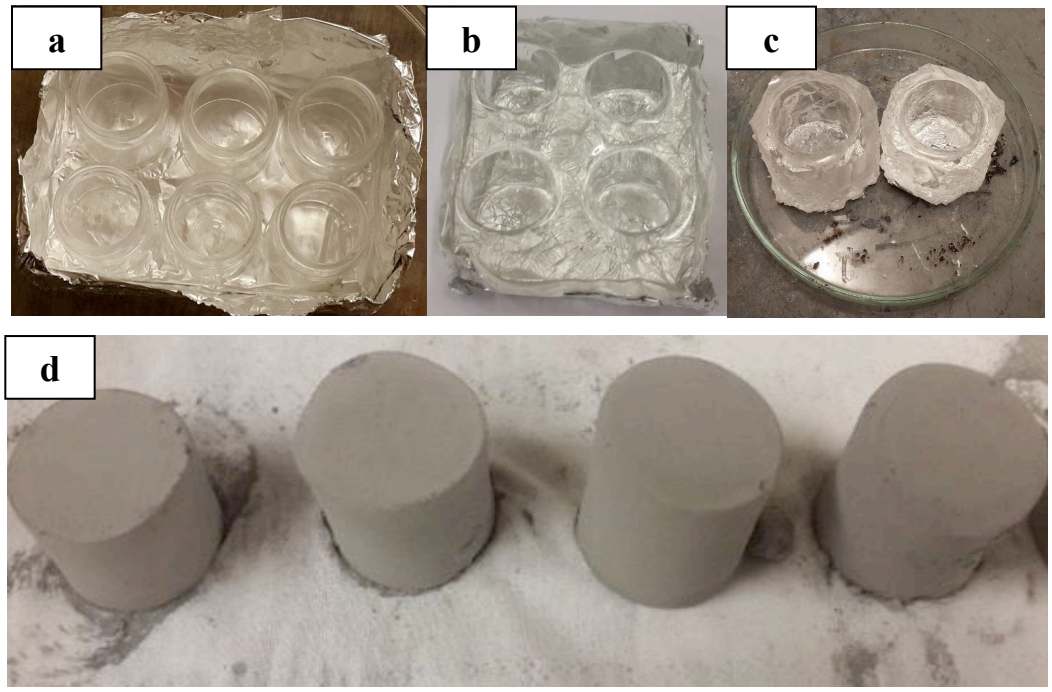

Figure 2. Preparation of the silicon rubber mould (a) the master mould, (b) the mould after casting and de-gassing, (c) samples of the rubber mould, (d) CIPed samples

B. CF-HIPing of the CIPed Disks

The CIPed compacts were subsequently HIPed using a capsule-free method (i.e. without any tooling or wrapping), as per the HIPing cycle shown in Figure 2. The cycle involved simultaneous application of temperature and pressure to 920˚C and 103 MPa, respectively, followed by an isothermal dwell at 920˚C of 2 hours, and finally furnace cooling at 5˚C/min, as described in previous work [20].

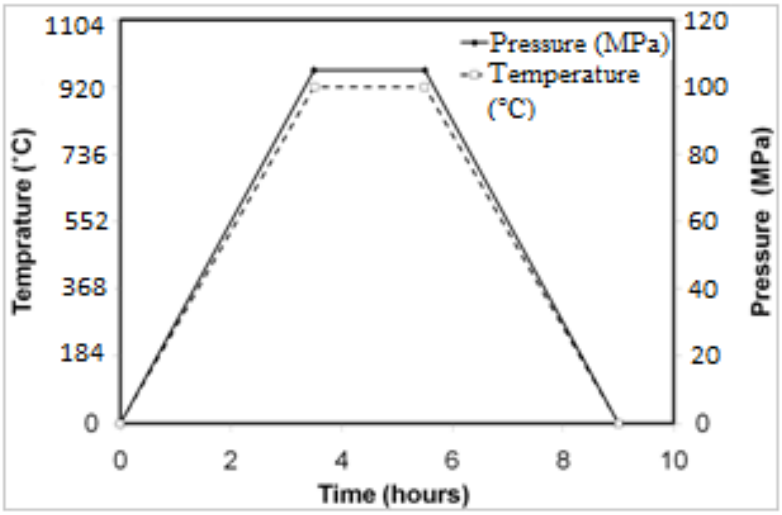

Figure 2. The used HIPing cycle for the consolidation of the capsule-free CIPed disks.

D. Microstructural Characterisation of the CF-HIPed Samples

The HIPed specimens were ground to remove at least 1 mm from the surface, followed by ultrasonic cleaning. The apparent density of the powder was measured using the hall flowmeter funnel of free flowing powder following the guidelines of ASTM B212 [21]. On the other hand, density of the green compacts was measured using the mass to volume ratio using the mass to volume ratio.

A Hitachi TM3000 scanning electron microscope (SEM) was used to characterise the microstructure. Micrographs from the CF-HIPed samples were taken at random locations across the polished sample surface. Quantitative image analysis (using ImageJ®) was used to quantify the porosity size and distribution. A JEOL7000 SEM, equipped with electron backscattered diffraction (EBSD), was used to study the effect of the particle size on the onset of consolidation. Furthermore, the samples were also scanned using a Bruker Skyscan1172 micro-computer tomography (micro-CT) system, with a maximum X-ray energy of 80 kV, 8 W beam power, 570 ms exposure per projection, aluminium and copper filter, and 3.4 µm pixel size to check the level of porosity within the HIPed samples. The scanned data were reconstructed into a 3-dimensional volume using NRecon Software (Bruker) [22], producing images with a spatial resolution of ~5 µm. Following reconstruction, the images analysis and thresholding were performed by CTan module (Bruker). 3D visualisation of surface connected and enclosed porosity was performed over selected volume of interest using CTVol module (Bruker). For all four samples region of

interest was selected across 1000 slices positioned in the middle of the longitudinal axis (y-axis) of the samples to create volume of interest.

Micro-hardness measurements were carried out on polished surfaces of the samples using an INDENTEC hardness tester with a Vickers indenter and using a load of 10 kg. In addition, compression test samples were machined out from the HIPed parts (5 samples per condition), with a square cross section of 5 mm × 5 mm and a length of 10 mm. The testing was performed using a ESH Servo Hydraulic Machine by applying a strain rate of 1 mm/min[1]. The average maximum strength of the samples, Young's modulus and ductility of the samples were determined using the stress strain diagram of each sample. The maximum strength was obtained as the maximum compressive strength, while the Young's modulus was calculated by dividing the stress over strain within the elastic region. Finally, the ductility of the samples was obtained using the maximum strain-to-failure.

3. RESULTS

Effect of the particle size on the apparent, CIPed, HIPed densities is shown in Table 2. As shown in the table, the apparent density was 41.4%, 47.2%, 50.3 and 53.5% for particle size 5 μm, 10 μm, 16 μm and 50 μm respectively. It can be noted that as the apparent density increases as the powder size increases as well. The mass of the samples was measured by an electronic balance. On the other hand, the volume of the CIPed samples size were calculated using $(V) = \pi/4 \times D^2 \times h$ where h and D are the height and the diameter, respectively. The density of the CIPed compacts was 54.1%, 58.0%, 60.2 and 63.1% for particle size 5 μm, 10 μm, 16 μm and 50 μm respectively. The CIPed density has increased with increasing the particle size. However, the CIPed density of the small particle size (5 μm) has increased by 12.7% while the CIPed density of the large particle size (50 μm) has increased by 9.6%.

Table 2: Apparent, CIPed, HIPed densities (relative to the theoretical density) of samples prepared using powders with mean particle size diameter of 5 μm, 10 μm, 16 μm, and 50 μm.

Particle size	Apparent density	CIPed density	HIPed Density
5 μm	41.4 %	54.1 %	98.6 %
10 μm	47.2 %	58.0 %	89 %

16 μm	50.3 %	60.2 %	87.1 %
50 μm	53.5 %	63.1 %	74.6 %

Figure 3 shows SEM images of the cross sections of the porous 316L samples following CF-HIPing of the CIPed compacts. The different samples show varying level of consolidation, caused by diffusion bonding between the powder particles, with the finest powder (Figure 3-a) showing the highest level of bonding between the powder particles due to the short diffusion paths, compared with the presence of open channels between the powder particles in the coarsest powder (Figure 3-d).

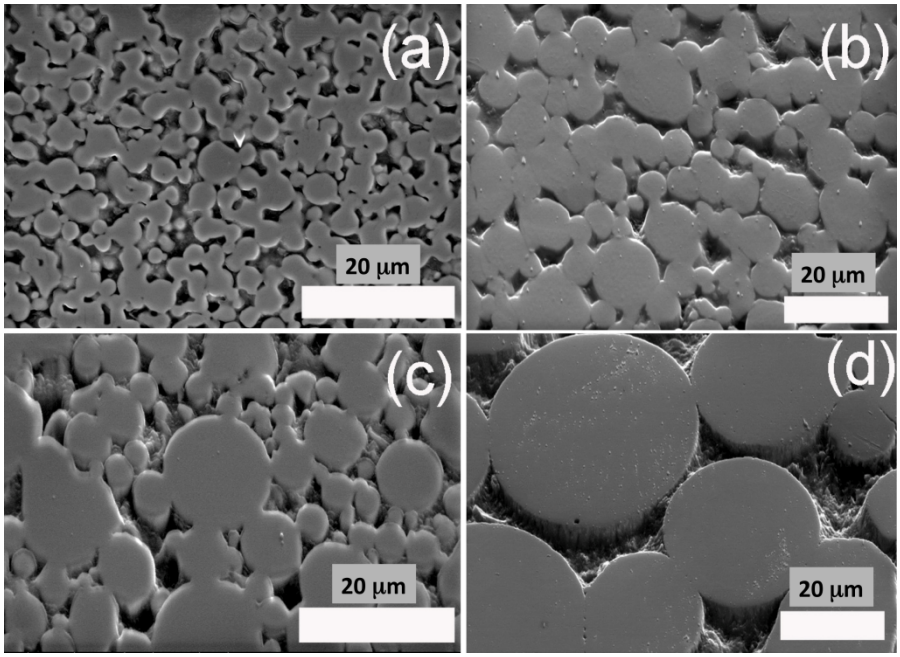

Figure 3: SEM micrographs of the cross sections of porous 316L CF-HIPed samples of different particle sizes: (a) 5 μm, (b) 10 μm, (c) 16 μm and (d) 50 μm.

The size of the channels between the particles generally increases with the increase in powder size. EBSD mapping was performed on the same regions (Figure 4), confirming the presence of significant bonding in the 5 μm and 10 μm samples, as well as the presence of recrystallisation twins within the powder particles. Conversely, limited bonding between the powder particles and presence of twins was observed in the 16 μm and 50 μm samples, Figures 4-c,d). It is clear that

the grain size within the particles (which is an outcome of the atomisation process), increases with the increase in the original particle size. As such, the mechanical properties of the CF-HIPed structures are likely to rely on the combination of the degree of consolidation (i.e. density of the consolidated component) and the grain size.

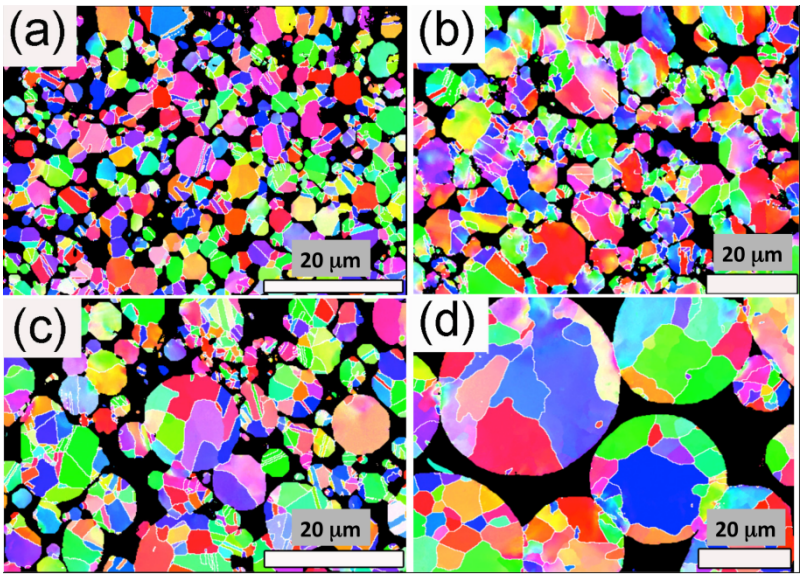

Figure 4: EBSD maps for the same regions identified in Figure 5, showing the cross sections of porous 316L CF-HIPed samples of different particle sizes: (a) 5 µm, (b) 10 µm, (c) 16 µm and (d) 50 µm.

To characterise the density of the CF-HIPed samples and the morphology of consolidation, micro-CT was performed to quantify the 3D variation in total porosity (surface connected and enclosed) using samples extracted from the core of the 4 conditions. In micro-CT, open porosity (surface connected) is described as any void found within a solid object or between solid parts, which has a connection to the surface outside the part. Closed porosity (enclosed) defined as a connected voids (black) voxels that is fully enclosed by solid (white) voxels. Total porosity, surface connected and enclosed pores have been distinguished, visualised and quantified (Table 3 and Figures 5). In addition, 3D volume renderings of the CF-HIPed samples are shown in Figure 6. Finally, the change of porosity level of the samples with increasing the powder particle size is

shown in Figure 7. The results show that porous structures can be achieved when coarse powder is used while a near fully dense condition using the CF-HIPing approach when using a fine powder size.

Table 3: Quantitative analysis of total, surface connected and enclosed porosity and pore size range within the 4 types of samples prepared with different particle size.

Particle size (µm)	**5**	**10**	**16**	**50**
Total porosity (%)	1.4	11.0	12.9	25.4
Surface connected porosity (%)	0.1	8.5	11.2	24.97
Enclosed porosity (%)	1.3	2.7	1.9	0.40
Pore size range (µm)	24- <78	10-<78	10-<57	10-<57

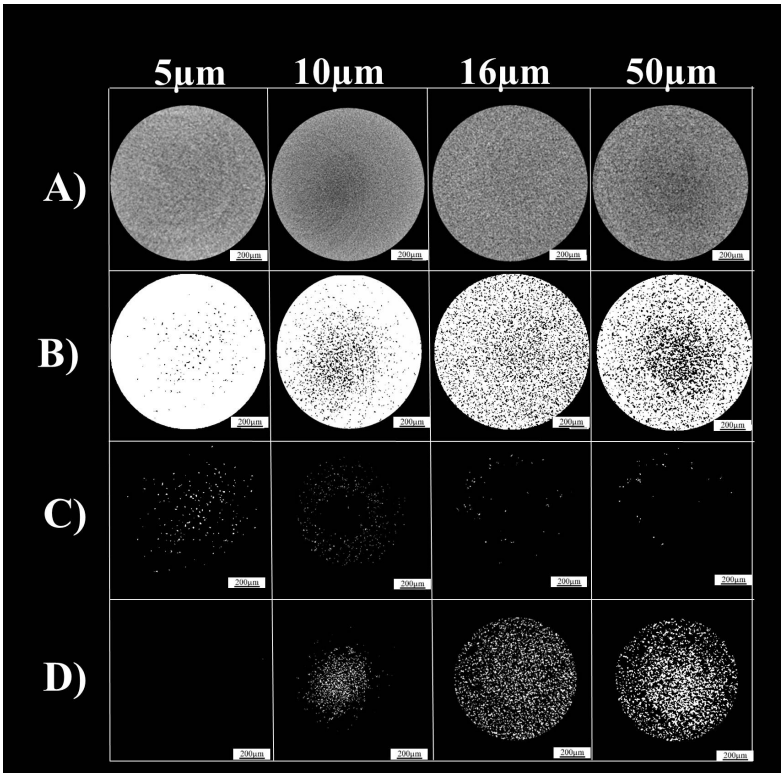

Figure 5. Representative cross-sectional micro-CT slice using A) grey scale, B) binarised view, C) binary enclosed porosity, and D) binary surface connected porosity in 316L CF-HIPed samples of the various particle sizes.

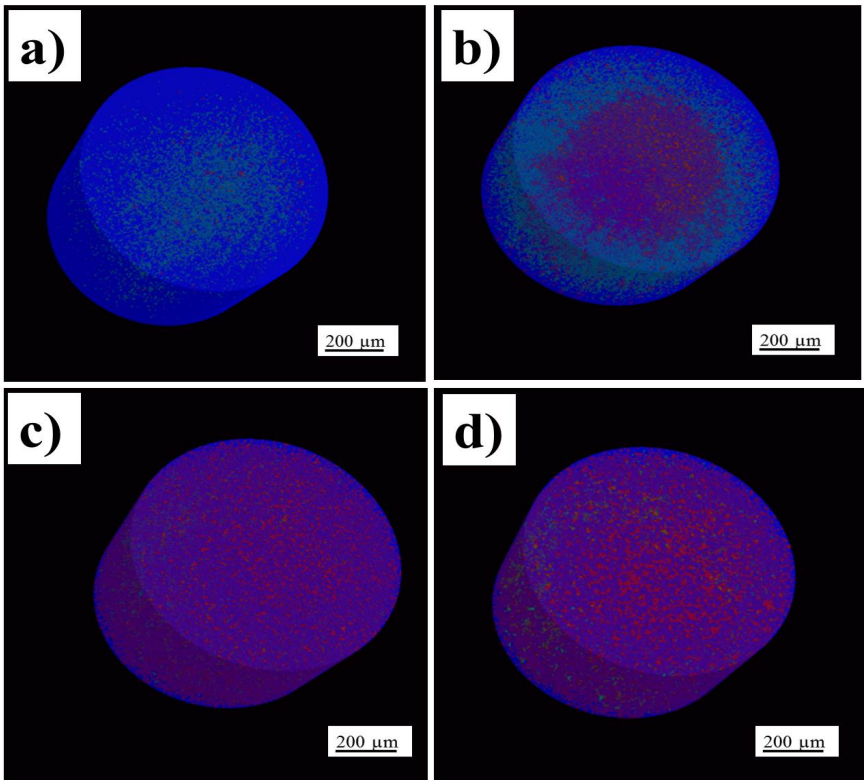

Figure 6. 3D visualization of open and closed porosity throughout the 316L HIPed samples prepared with various particle size of a)5 µm, b)10 µm, c)16 µm and d) 50 µm indicating the increase of level of open porosity when the particle size of starting material increase. Blue= total volume of interest, Green=closed porosity and red= open porosity.

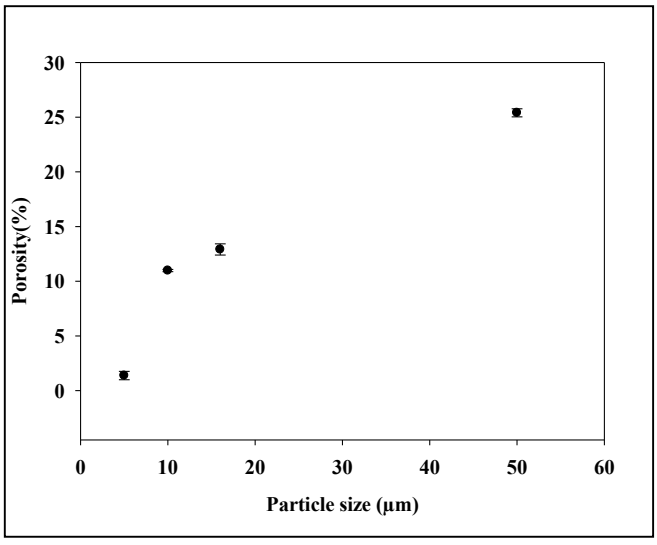

Figure 7. The relationship between powder particle size and pore fraction in the 316L CF-HIPed samples.

It is known that HIPing cannot consolidate surface connected pores. As such, it is useful to visualise the effectiveness of the CIPing stage in sealing the internal pores via examining the surface of the CF-HIPing compacts. As shown in Figure 8, the surface of the samples revealed a highly porous surface, with porosity approaching 30-50% in the 4 conditions. The depth of the porous region varied from ~80 μm in the 5 μm powder size, to 350 μm for the 50 μm powder size. However, within the compact itself, the pore fraction increased to the ranges identified by microCT (Table 3).

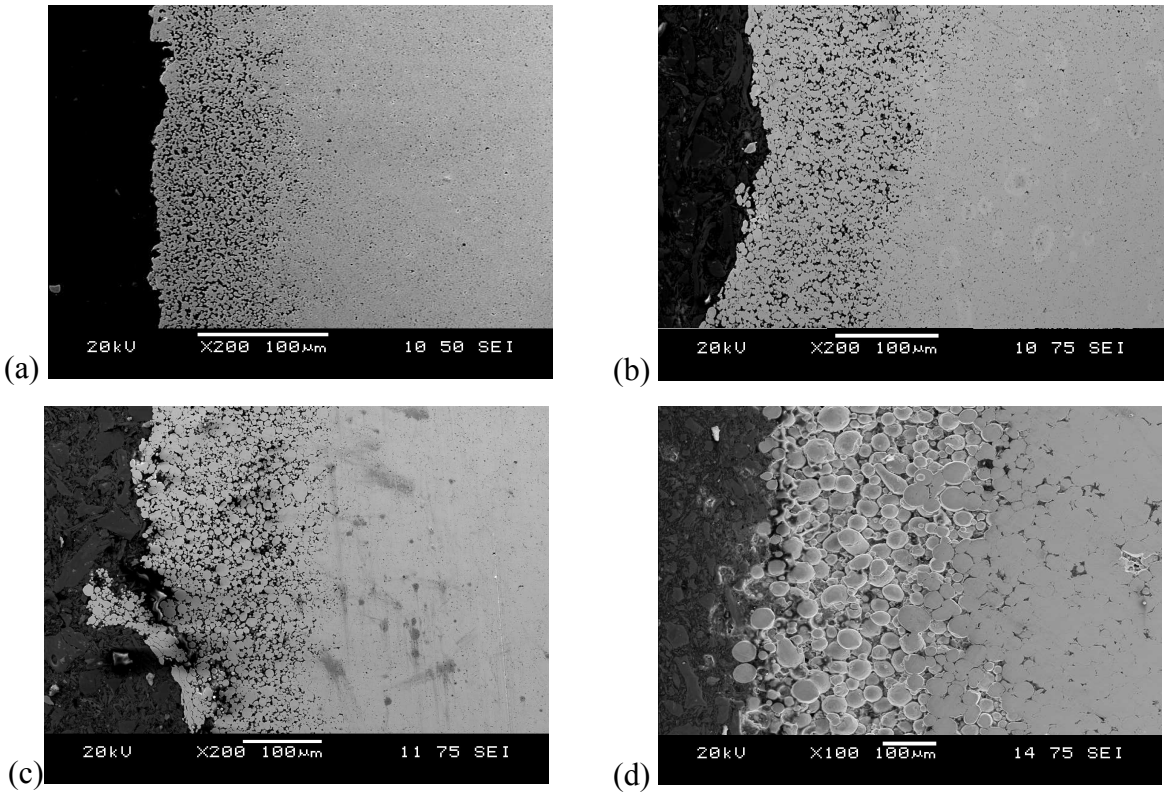

Figure 8**.** Morphology of the surface layer of the 316L HIPed samples prepared with various particle size of a)5 μm, b)10 μm, c)16 μm and d) 50 μm

Figures 9 show the influence of the particle size on Young's modulus, compressive strength, ductility and macro-hardness of the CF-HIPed samples. In general, all these properties (in addition to the density) decrease with the increase in particle size. Samples with particle size of 5 μm showed the highest combination of mechanical properties (Young's modulus of 50 GPa, 360 MPa ultimate compressive strength, 40% ductility, and 49 HV hardness). Conversely, increasing the particle size to 50 μm was accompanied by an obvious decline in the mechanical properties to reach 17 GPa, 108 MPa, 17%, and 25 HV, for the Young's modulus, ultimate compressive strength, ductility, and hardness, respectively. As explained the particle size of the powder has a significant effect on the morphology of the pores and the porosity fraction, in addition to the grain size within the powder particles, which is an outcome of the atomisation process. In turn, these factors control the mechanical characteristics of the HIPed materials. It could be clearly shown from Figures 9 and 10 that as the particle size increases the porosity % increases which has a detrimental influence on the mechanical properties of the material. The best approach is to optimise Young's modulus-to-porosity% ratio to match bone properties through using a particle size that could produce the desired values for the Young's modulus and porosity%. Based upon the presented results, stainless steel implants prepared using particle size ranges from 32-50 μm would produce samples with Young's modulus ranges between 17-30 GPa and porosity ranges between 17-25 %, as shown in Figure 10. At this condition, the compressive strength, ductility and hardness would be 107-190 MPa, 17-26% and 25-28 HV, respectively.

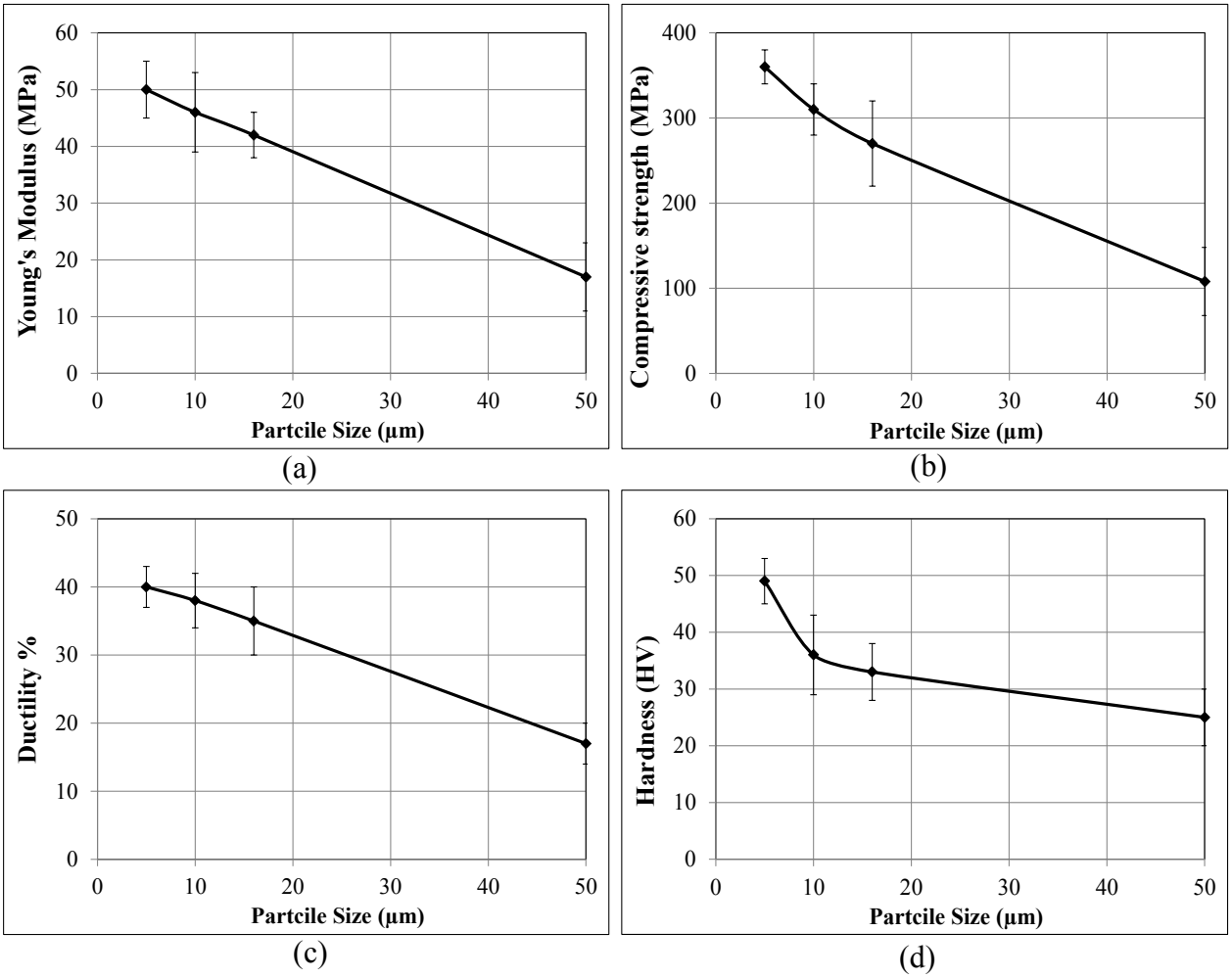

Figure 9. The effect of powder particle size on the mechanical properties of 316L HIPed samples, (a) Young's modulus, (b) Compressive strength, (c) Ductility and (d) Macro hardness.

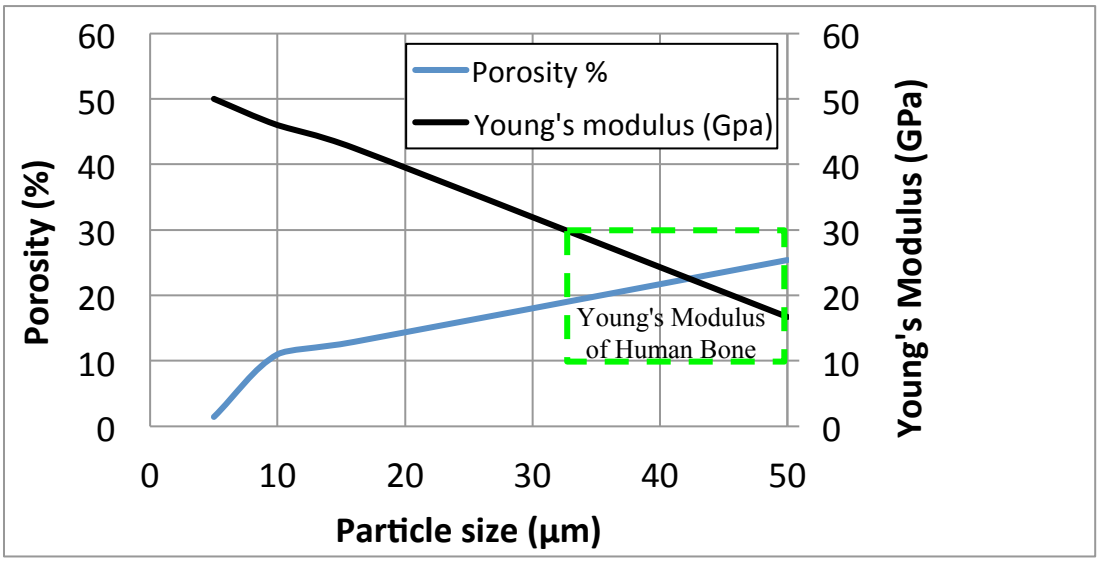

Figure 10. Recommended particle size for optimum values of porosity and Young's modulus

4. DISCUSSION

During CF-HIPing of stainless steel 316L, the powder is consolidated by solid-state diffusion, affecting the porosity content, morphology, size, and pore distributions, which were all found in this study to be significantly dependent on the powder particle size, especially when CIPing CF-HIPing parameters (pressure, temperature, and hold time) were all kept constant. This was verified using micro-CT imaging and cross-sectional SEM micrographs. There is generally an increase in the volume fraction of porosity, the average pore size, and the level of interconnectivity between the porosity networks with the increase in the particle size increases the amount of porosity as well as the average pore size increases. In addition, there was a noticeable increase the irregularity of the shape of the pores and their interconnectivity as a result of the increasing particle size.

The differences in the total porosity, pore size and pore morphology are highly related to the densification mechanism during CF-HIPing. The samples used in the current study were HIPed at a temperature 920˚C and a pressure of 103 MPa. On the other hand, the typical sintering temperature of 316L is about 1200˚C, with the densification typically occurring at a temperature of 900˚C [23]. Therefore, densification during sintering is one of the contributors to increase the density of the samples compacts during CF-HIPing. As the compacts were formed using different particle sizes, porosity of the samples was found to increase with the increase of the particle size. This is in agreement with the results presented by Choi *et al.* [23], who reported an increase in the density with the decreasing of 316L particle size. On the other hand, the pressure of the inert gas during CF-HIPing has both densification and anti-densification mechanisms. During HIPing, the particles are plastically deformed due to the action of the high temperature and pressure. Hence, the density is increased. On the other hand, the presence and the expansion of the trapped gas in the pores during CF-HIPing act as a densification resistance factor. CIPed samples with coarse particle size have larger and more interconnected pores, while CIPed samples with small particle size have smaller and less interconnected pores. Therefore, the densification resistance factor of the trapped gas pressure in the pores is more significant for samples prepared using coarse particle size.

As shown in Figures 3 (d) and 4 (d), the amount of pores was much higher when compared to the other three samples. High amount of open porosity defines the excellent interconnectivity in that

sample. Also, it is clearly shown that most of the pores in this sample are interconnected, which is preferable to improve the transportation of body fluid and hence enhance the growing of tissues around the implant. This was in agreement with the results by Bhattari *et al.*, [24] who showed an improved performance of the dental implants in vivo with the materials of high porosity which allowed for an enhanced bone healing and long term maintenance of osseointegration.

Quantitative analysis of the porosity demonstrated the porosity level increased by ~ 18 fold from 1.4% to 25% with the increase in the mean particle size from 5 μm to 50 μm. From Figure 7 it can be noted that the surface connected porosity level within all samples increased as a result of increasing particle size. 3D visualization of surface connected and enclosed porosity throughout all four samples (Figure 8) also illustrates the porosity within the samples was predominantly surface connected (red colour). In this study Larger stainless particle size resulted in significant increase (>90% of total porosity) in surface connected /interconnected porosity throughout the samples (Figure 8d- covered with red colour) indicating the potential of this method for production of three-dimensional implant with interconnected porosities that may be suitable for bone tissue.

It could be speculated that depending on the particle size of the starting materials, different forms of stainless steel parts with various porosity levels (surface connected and enclosed pores) have been produced. Highly interconnected porosity features have two main advantages in bone implant design; 1) to direct cell growth and support vascularization of the ingrown tissue as well as 2) the structure can be tuned to match the implant stiffness to the surrounding tissues reducing stress-shielding effects [25, 26].

It could be inferred from the optical micrographs that the irregular pore formation, large pore size and high pore fraction, which are associated with the increased particle size, caused all the mechanical properties examined in this study to decrease. This confirmed the results by Kurgan [1] and Dewidar [27] who reported a remarkable drop in the properties of the sintered samples as a result of the increased porosity level. Furthermore, another study by Leyens and Peters recommended that the porosity of an implant made from titanium alloys should be about 20% in order to obtain satisfactory mechanical and biological properties [28]. In the current study, 1.4 % porosity 316L stainless steel implants could be achieved using particle size of 5 μm, which showed the best properties when compared to the rest of the samples. The compressive strength

of that samples was about 360 MPa which exceeds that of a bulk base metal [29]. Additionally, a higher porosity content of about 25.4 % (related to particle size of 50 μm), resulted in a young's modulus of 17 GPa, which is appropriate for medical implants applications [5, 7, 8].

The presence of the surface porosity shown in Figure 8 has two interesting aspects to note. First, surface porosity will be beneficial for osseointegration, combined with the bulk porosity which will give a lower modulus for the part, and thus enhancing the biomechanical compatibility of the implant. Second, if CF-HIPing route is to be used for netshape HIPing to create solid dense structures, it can be foreseen that a near netshape component can be produced using this route, with only limited surface machining (in the order of <500 μm) will be required to remove the surface connected layer.

5. CONCLUSIONS

The present study demonstrated that controlled porosity stainless steel parts can be fabricated by a combination of CIPing and CF-HIPing. The effect of the powder particle size on densification behaviour, microstructure and mechanical properties were studied. The following conclusions could be drawn:

1. The proposed approach can be used to fabricate samples which are appropriate for hard-tissue applications with Young's moduli between 17 and 30 GPa were successfully fabricated. The porosity fraction for those samples was 16 to 25.4% and the mechanical properties were 107 to 190 GPa for compressive strength, 17 to 26% for ductility and from 25 to 28 HV for macro-hardness.
2. Decreasing the powder particle size resulted in an improvement of the Young's modulus, compressive strength, ductility, and macro-hardness of the 316L CF-HIPed samples.
3. The HIPed stainless steel samples of particle size between 5 and 50 μm had a porosity level varying from 1.4% to 25.4%, respectively.
4. The pore characteristic, e.g. pore shape, size and distribution, of the CF-HIPed samples can be optimised by controlling the particle size of the powder.
5. Although the aim of this work was mainly to develop porous structures, the results highlight the possibility of using the CF-HIPing approach to create highly dense structures, when a fine particle size is used. This limits the degree of surface connectivity, leaving behind a porous surface region of ~100 μm, which can be later machined or electrochemically etched to generate a fully dense surface.
6. The study focused on the effect of the effect of the particle size on the porosity, the microstructure and the mechanical properties of the CF-HIPing samples. Effect of other parameters such as the CIP, HIP conditions, and sample size should be considered in future work.

References

[1] N. Kurgan, Effect of porosity and density on the mechanical and microstructural properties of sintered 316L stainless steel implant materials, Materials & Design 55 (2014) 235-241.
[2] R. Fujisawa, M. Sakaihara, Y. Kurata, Y. Watanabe, Corrosion behaviour of nickel base alloys and 316 stainless steel in supercritical water under alkaline conditions, Corrosion Engineering, Science and Technology 40(3) (2005) 244-248.
[3] K.J. M. Imbaby, and I. Chang, Net shape fabrication of stainless-steel micro machine components from metallic powder, Journal of Micromechanics and Microengineering 18(11) (2008) 115018 (115017 pp.).
[4] K. Essa, F. Modica, M. Imbaby, M.A. El-Sayed, A. ElShaer, K. Jiang, H. Hassanin, Manufacturing of metallic micro-components using hybrid soft lithography and micro-electrical discharge machining, The International Journal of Advanced Manufacturing Technology 91(1) (2017) 445-452.
[5] S. Bender, V. Chalivendra, N. Rahbar, S. El Wakil, Mechanical characterization and modeling of graded porous stainless steel specimens for possible bone implant applications, International Journal of Engineering Science 53 (2012) 67-73.
[6] M.M. Dewidar, K.A. Khalil, J.K. Lim, Processing and mechanical properties of porous 316L stainless steel for biomedical applications, Transactions of Nonferrous Metals Society of China 17(3) (2007) 468-473.
[7] A. Bandyopadhyay, F. Espana, V.K. Balla, S. Bose, Y. Ohgami, N.M. Davies, Influence of porosity on mechanical properties and in vivo response of Ti6Al4V implants, Acta Biomaterialia 6(4) (2010) 1640-1648.
[8] F.E. Wiria, J.Y.M. Shyan, P.N. Lim, F.G.C. Wen, J.F. Yeo, T. Cao, Printing of Titanium implant prototype, Materials & Design 31, Supplement 1 (2010) S101-S105.
[9] A. Fathy, A. Ahmed, H. Morgan, Characterization and optimization of steel foam produced by slip casting process, MetFoam 2007 - Proceedings of the 5th International Conference on Porous Metals and Metallic Foams, 2008, pp. 161-164.
[10] L.P. Lefebvre, M. Gauthier, M. Patry, Processing and properties of iron-based metallic foams, Advances in Powder Metallurgy and Particulate Materials - 2005, Proceedings of the 2005 International Conference on Powder Metallurgy and Particulate Materials, PowderMet 2005, 2005, pp. 136-148.
[11] C. Qiu, S. Yue, N.J. Adkins, M. Ward, H. Hassanin, P.D. Lee, P.J. Withers, M.M. Attallah, Influence of processing conditions on strut structure and compressive properties of cellular lattice structures fabricated by selective laser melting, Materials Science and Engineering: A 628 (2015) 188-197.
[12] K. Essa, H. Hassanin, M. Attallah, N. Adkins, A. Musker, G. Roberts, N. Tenev, M. Smith, Development and Testing of an Additively Manufactured Monolithic Catalyst Bed for HTP Thruster Applications, Applied Catalysis A: General (2017).
[13] H. Hassanin, K. Essa, C. Qiu, A.M. Abdelhafeez, N.J. Adkins, M.M. Attallah, Net-shape manufacturing using hybrid selective laser melting/hot isostatic pressing, Rapid Prototyping Journal 23(4) (2017).
[14] H.V. Atkinson, S. Davies, Fundamental aspects of hot isostatic pressing: An overview, Metall and Mat Trans A 31(12) (2000) 2981-3000.
[15] M.H. Bocanegra-Bernal, Hot Isostatic Pressing (HIP) technology and its applications to metals and ceramics, Journal of Materials Science 39(21) (2004) 6399-6420.
[16] K.T. Kim, Y.C. Jeon, Densification behavior of 316L stainless steel powder under high temperature, Materials Science and Engineering: A 245(1) (1998) 64-71.
[17] A. Abdelhafeez, K. Essa, Influences of Powder Compaction Constitutive Models on the Finite Element Simulation of Hot Isostatic Pressing, Procedia CIRP 55 (2016) 188-193.

[18] C. Qiu, N.J.E. Adkins, H. Hassanin, M.M. Attallah, K. Essa, In-situ shelling via selective laser melting: Modelling and microstructural characterisation, Materials & Design 87 (2015) 845-853.
[19] K. Essa, R. Khan, H. Hassanin, M.M. Attallah, R. Reed, An iterative approach of hot isostatic pressing tooling design for net-shape IN718 superalloy parts, Int J Adv Manuf Technol 83(9–12) (2016) 1835-1845.
[20] S. Irukuvarghula, H. Hassanin, C. Cayron, M.M. Attallah, D. Stewart, M. Preuss, Evolution of grain boundary network topology in 316L austenitic stainless steel during powder hot isostatic pressing, Acta Materialia 133(Supplement C) (2017) 269-281.
[21] ASTM B212-09, "Standard test method for apparent density of free-flowing metal powders using the hall flowmeter funnel," 2008.
[22] NRecon, SkyScan/Bruker micro-CT, Kartuizerweg 3B 2550 Kontich, Belgium,, 2011.

[23] J.-P. Choi, G.-Y. Lee, J.-I. Song, W.-S. Lee, J.-S. Lee, Sintering behavior of 316L stainless steel micro–nanopowder compact fabricated by powder injection molding, Powder Technology 279(Supplement C) (2015) 196-202.
[24] S.R. Bhattarai, K.A.-R. Khalil, M. Dewidar, P.H. Hwang, H.K. Yi, H.Y. Kim, Novel production method and in-vitro cell compatibility of porous Ti-6Al-4V alloy disk for hard tissue engineering, Journal of Biomedical Materials Research Part A 86A(2) (2008) 289-299.
[25] R. Singh, P. Lee, T. Lindley, C. Kohlhauser, C. Hellmich, M. Bram, T. Imwinkelried, R. Dashwood, Characterization of the deformation behavior of intermediate porosity interconnected Ti foams using micro-computed tomography and direct finite element modeling, Acta biomaterialia 6(6) (2010) 2342-2351.
[26] K. Rezwan, Q. Chen, J. Blaker, A.R. Boccaccini, Biodegradable and bioactive porous polymer/inorganic composite scaffolds for bone tissue engineering, Biomaterials 27(18) (2006) 3413-3431.
[27] M. Dewidar, Influence of processing parameters and sintering atmosphere on the mechanical properties and microstructure of porous 316L stainless steel for possible hard-tissue applications, International Journal of Mechanical and Mechanics Engineering 12(1) (2012) 10-24.
[28] J. Breme, E. Eisenbarth, V. Biehl, Titanium and its Alloys for Medical Applications, Titanium and Titanium Alloys, Wiley-VCH Verlag GmbH & Co. KGaA2005, pp. 423-451.
[29] AZONwtwork, http://www.azom.com/properties.aspx?ArticleID=863, 2000-2015. (Accessed 28/8 2015).